Biosensors and Bioelectronics 148 (2020) 111809

Contents lists available at ScienceDirect

Biosensors and Bioelectronics

journal homepage: http://www.elsevier.com/locate/bios

A multiple mixed TiO_2 mesocrystal junction based PEC-colorimetric immunoassay for specific recognition of lipolysis stimulated lipoprotein receptor

Yanjie Chen [a], Shupei Zhang [b], Hong Dai [a,b,*], Zhensheng Hong [a], Yanyu Lin [b]

[a] College of Chemistry and Materials, Fujian Normal University, Fuzhou, Fujian, 350108, China
[b] Fujian Provincial Maternity and Children's Hospital, Affiliated Hospital of Fujian Medical University, Fuzhou, Fujian, 350108, China

ARTICLE INFO

Keywords:
MMMJ
Cu nanoclusters
PEC immunoassay
Digital colorimetric assay
Lipolysis stimulated lipoprotein receptor

ABSTRACT

A flexible two-step photoelectrochemical (PEC)–colorimetric immunoassay was proposed for ultrasensitive detection of lipolysis stimulated lipoprotein receptor (LSR) which is found to be closely related to ovarian cancer (OC). In this paper, the Cu nanoclusters (CuNCs) enhanced multiple mixed TiO_2 mesocrystals junction (MMMJ) was fabricated via effective combination of multiple different phases TiO_2 mesocrystals (Anatase and Rutile) layers and used as a sensing platform. The strong interaction between different phases layers caused multiple amplification of signal and introduction of Cu NCs further improve PEC properties and catalytic activity to hydrogen peroxide (H_2O_2) what can catalyze lecuo-methylene blue (lecuo-MB) from colorless to blue. As antibody and target antigen captured onto the MMMJ in turn, both PEC properties and catalytic activities were inhibited, leading to decreased photocurrent responses and multiply vivid color variations in lecuo-MB functionalized colorimetric films. Thus, a versatile dual-modal sensing system was developed just by utilizing enhanced MMMJ as a photoelectrode and lecuo-MB as a color change reporter molecule for PEC and colorimetric monitoring of target. Combing all of these advantages, the designed dual-modal immunoassay considerately reduced false positive or negative results during the measurement, and the unique approach for MMMJ construction may also provide a valuable guidance for designing other mixed phase junctions with superior PEC performance.

1. Introduction

Ovarian cancer (OC) is the most common gynecological malignant tumor with highest mortality, every year nearly 200,000 women are diagnosed with ovarian cancer all over the world (Shinagare et al., 2018). According to previous research, survival rate of advanced stage OC was approximately 30%. While the 5-year survival rate can up to more than 90% when OC was diagnosed at early state, which motivated more researches to explore early diagnostic biomarkers for OC monitoring (Su et al., 2013). Fortunately, the lipolysis stimulated lipoprotein receptor (LSR) as a lipid metabolism regulating protein always shows significant effect on the lipid environment especially in women ovarian. Therefore, LSR was considered to be closely related to some malignant diseases such as OC. Up to now, there have some researches tried to confirm that LSR was implicated in the pathogenesis of OC and may be utilized as a new biomarker for OC early prediction (Hiramatsu et al., 2018). While currently the quantitative analysis for LSR detection have not established. Accordingly, in this work, an innovative method was developed to realize sensitive and accurate determination of LSR.

Photoelectrochemical (PEC) measurement as a newly emerged and exuberantly developing technique with specific bio-affinity properties and inherent sensitivity has attracted considerable scholarly attention. In the PEC sensing platform, proper photoactive materials and constructing strategy always played key roles. Thereinto, a mixed heterojunction composed of two different phases with one semiconductor anatase/rutile TiO_2 heterojunction displayed strengthened PEC properties and extensively applied because of internal electric field between different phases could significantly accelerated the electron-hole separation (Yan et al., 2018). While most anatase/rutile TiO_2 heterojunction suffered from complex making progress and frequently involved high pressure, high temperature, which cost long periods of time and may even lead to collapse of lattice structure. In this case, a unique multiple

* Corresponding author. College of Chemistry and Materials, Fujian Normal University, Fuzhou, Fujian, 350108, China.
E-mail address: dhong@fjnu.edu.cn (H. Dai).

https://doi.org/10.1016/j.bios.2019.111809
Received 15 August 2019; Received in revised form 8 October 2019; Accepted 21 October 2019
Available online 26 October 2019

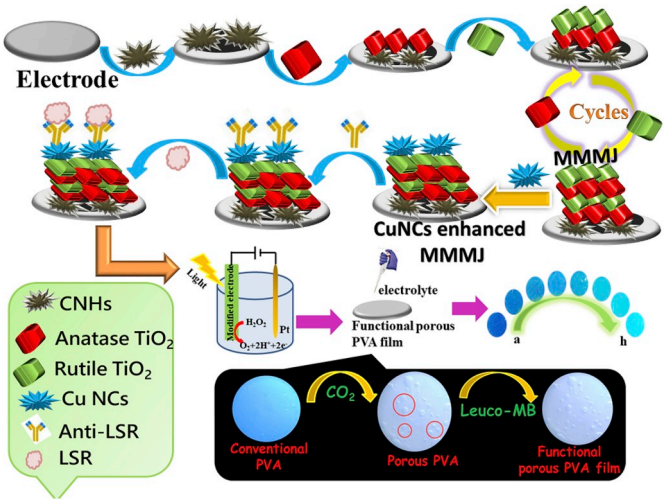

Scheme 1. The illustration of the construction process of PEC biosensor.

mixed TiO_2 mesocrystals junction (MMMJ) was fabricated just through overlap of multiply different phases TiO_2 mesocrystals (Anatase and Rutile) layers at room temperature without any complex instrument, which overcame the defects of low synthesis efficiency, high cost and minimized the damage to lattice structure as much as possible (Dai et al., 2014, 2015; Liu et al., 2016). Moreover, the strong interaction between different phase layers caused multiple amplification of signal to generate more brilliant photocurrent response. The staggered band gap between different phase layers lead to formation of favorable built-in potential distribution in MMMJ, which drove electrons and holes toward the desired direction (Cao et al., 2016; Jia et al., 2018; Su et al., 2011). And aligned conductive bands in MMMJ facile electrons migrate on different phases layers to remarkably prolonged the electrons life time (Zhang and Dong, 2019).

The Cu NCs as a new kind of nanomaterials CuNCs consisting of tens of small size atoms possess good biocompatibility, excellent photostability, low cost and facile to prepare. Cu NCs play a critical role in strengthening PEC and catalytic properties of MMMJ for small size atoms provided higher surface areas to promote reaction activity. And discrete energy levels and confined electrons of atoms in molecular dimensions could also dramatically improved electronic and optical properties (Jin et al., 2015; Cui et al., 2014). Moreover, it was widely known that the LSPR effect of Cu NCs caused enhanced the electric near-field around the metals which can effectively suppress recombination of electron-hole pairs by trapping electrons from MMMJ (Liu et al., 2015). Combine all of these advantages, Cu NCs would be utilized as an ideal sensitization agent to further promote PEC performance in MMMJ.

Impressively, the fabricated CuNCs enhanced MMMJ also found to have excellent catalytic activity to H_2O_2, what can oxidize lecuo-MB (as a color change reporter molecule) from colorless to deep blue (Ren et al., 2017; Hao et al., 2016; Ding et al., 2018). However, after H_2O_2 was decomposed by enhanced MMMJ, the oxidation of lecuo-MB was suppressed. Therefore, a color intensity variation in lecuo-MB functionalized colorimetric films could be observed when treated with H_2O_2 at different concentration. Moreover, conventional colorimetric detection method only rely on naked eyes were susceptible to variation in the user's interpretation. On the basic of this, a more accurate digital colorimetric analysis was established by transforming the raw photograph of colorimetric film into RGB image. The color intensity value (Red, Green and Blue) in different films could be record to have an accurate digital evaluate, which provided an important reference for PEC measurement and effectively avoid the false results during the analysis. (Kalinichev et al., 2019; Wei et al., 2018).

Herein, a robust two-step PEC-colorimetric immunoassay was designed for accurate detection of LSR by using an enhanced MMMJ as a sensing substrate. The detail progress was described in Scheme 1, MMMJ was first constructed just by deposing two different phases TiO_2 mesocrystals onto the carbon nanohorns (CNHs) modified electrode layer by layer and dried under infrared lamp. Next, the Cu NCs was introduced as sensitizer to further enhance the PEC performance in MMMJ (Miao et al., 2018; Liu and Zhu, 2013). The CuNCs enhanced MMMJ generated brilliant photocurrent response and exhibited outstanding catalytic activity to H_2O_2. After antigen recognized onto the electrode interface, both photocurrent response and catalytic activity were suppressed, caused a decreased photocurrent output and vivid color variations in colorimetric films. Benefiting from different mechanisms and independent signal transduction, the proposed dual-modal strategy not only presented outstanding sensitivity and satisfied specificity but also paved a promising path for detection of other biomarkers.

2. Experimental section

2.1. Material

Lipolysis stimulated lipoprotein receptor (LSR) and LSR polyclonal antibody were acquired from San Ying Biotechnology (Wuhan, China). Humanepididymisprotein 4 (HE4), α-fetoprotein (AFP), Human papillomavirus 16 E6 (HPV16 E6) and bovine serum albumin (BSA, 96–99%) were purchased from Bioss Inc (Beijing, China). The human serum sample were acquired from affiliated hospital of Fujian medical university (Fuzhou, China). Sodium dodecylbenzene sulfonate (SDBS), titanium (IV) isopropoxide (TIP), poly (vinyl alcohol) (PVA) and 4-Mercaptophenylboronic acid (4-MPBA) were all harvested from Aladdin Co. Ltd. (Shanghai, China). N-hydroxy succinimide (NHS) and 1-ethyl-3-(3-di-methylaminopropyl) carbodiimide hydrochloride (EDC) were obtained from Shanghai Medpep Co. (Shanghai, China). Yeast extract was from Angel Yeast Co. (Shanghai, China). Copper chloride ($CuCl_2$) and Glycerin were received from Sinopham Chemical Reagent Co. (Shanghai, China). Methylene blue (MB) was purchased from Sigma-Aldrich (China). The EDC/NHS solution was prepared by mixing 20 mM EDC and 10 mM NHS with volume ratio of 4:1. The Leuco-MB solution was perpared by mixing 10 mL of 0.1 M ascorbic acid (AA) and 3 mL of 1 mM (methylene blue) MB solution at room temperature until the color change from blue to colorless. The phosphate buffer solution (PBS) was prepared by mixing a stock solution of 0.1 M NaH_2PO_4 and 0.1 M Na_2HPO_4 and adjusting the pH value. And other reagents from Sinopham Chemical Reagent Co. (Shanghai, China) were analytical grade without further treatment. Ultrapure water (18.2 MΩ cm^{-1} at 25 °C) for all experiments was purified with Milli-Q Advantage water treatment system.

2.2. Apparatus

Open circuit potential (OCP), amperometric I-t curves, linear sweep voltammetry (LSV) and electrochemical impedance spectroscopy (EIS) were measured on CHI 760C electrochemical workstation (Shanghai Chenhua Instrument Co., China) with a conventional three-electrode system: Ag/AgCl electrode (sat. KCl) as the reference, a modified indium–tin-oxide electrode (ITO) (geometric area was 10 cm^2) as working electrode, and platinum (Pt) wire as auxiliary electrode. The pH value was measured on a PHS-3C exact digital pH meter (Leici Co.,Ltd., Shanghai, China). All the PEC measurements were performed at an applied potential of 0.1V in PBS (pH 7.5). The electrochemical impedance were determined in mixed solution of 5.0 mM $K_3[Fe(CN)_6]/K_4[Fe(CN)_6]$ (1:1) containing 0.1 M KCl. Additionally, a xenon lamp (86 $mWcm^{-2}$, Beijing, China) was utilized as the irradiation source and was filtered by monochromator before using. Scanning electron microscopy (SEM, S8010 instrument) and transmission electron microscopy (TEM, FEI F20 S-TWIN instrument) were used for the morphological and structural characterization of synthesized materials. X-ray diffraction

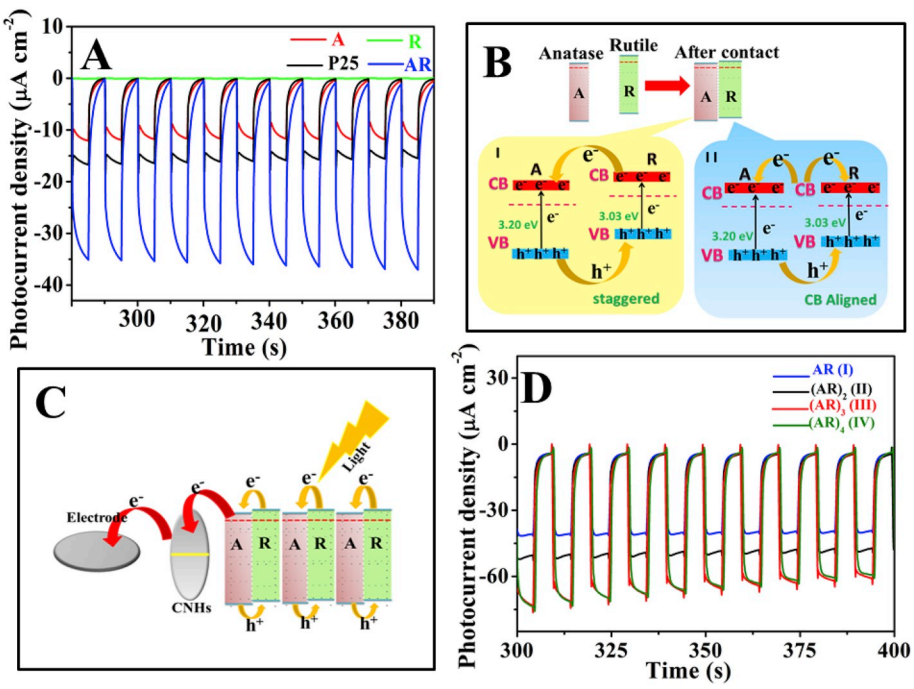

Fig. 1. (A) The photocurrent measurement of AnataseTiO_2 mesocrystals (red line), RutileTiO_2 mesocrystals (green line), P25 (black line) and Anatase/RutileTiO_2 mesocrystals junction (AR) (blue line) modified electrode. (B) Photocurrent generation mechanism in Anatase/Rutile TiO_2 mesocrystals junction (C) The excited electrons transfer regulation in MMMJ (D) The photocurrent responses in electrodes with different coating layers of Anatase/RutileTiO_2 mesocrystals junction (AR), AR (blue line), $(AR)_2$ (black line), $(AR)_3$ (green line), $(AR)_4$ (red line) in PBS (pH 7.5) with applied potential of 0.1 V. (For interpretation of the references to color in this figure legend, the reader is referred to the Web version of this article.)

(XRD) patterns were recorded on a PANalytical X'Pert spectrometer using Co Kα radiation (1.78897 Å), and the data were changed to Cu Kα data. Fluorescence spectroscopy were measured with Edinburgh FLS920 dedicated Fluorescence Spectrometer.

2.3. Synthesis and functionalization of Cu NCs

Prior to use, all glassware must be rinsed in a bath of freshly prepared 3:1 HCl/HNO_3 and thoroughly cleaned in ultrapure water. According to pervious report (Jin et al., 2016),[31] the yeast extract solution (8 mL, 100 mg) and $CuCl_2$ (2 mL, 100 mM) were mixed together and stirred for 2–3 min at room temperature. Next, the mixture was refluxed for 12 h at 100 °C until the color changed from light blue to deep green. Afterwards, the result solution was purified by centrifuging 10 min (10,000 r/min) to remove the solid from supernatant. The synthesized Cu NCs solution (0.25 mg mL^{-1}) was diluted into 0.20 mg mL^{-1} and stored at 4 °C for use. After that, 0.20 mg mL^{-1} Cu NCs solution and 0.2 mM 4-MPBA were mixed together with a volume ratio of 4:1 and shaking for 6 h to have an affinity reaction take place between Cu NCs and 4-MPBA via Cu-SH bond.

2.4. Construction of MMMJ sensing platform

The MMMJ structures were fabricated on clean ITO electrodes which were washed with anhydrous alcohol and ultrapure water in an ultrasonic bath and dried in air. Prior to modification, a layer of insulated tape with uniform holes (diameter was 3 mm) was pasted onto the bare ITO electrodes surface. After that, as illustrated in Scheme 1, 5 μL of 3 mg mL^{-1} CNHs suspension was firstly dropped on each holes and dried under infrared lamp. Next, 5 μL of 3 mg mL^{-1} anatase TiO_2 mesocrystals suspension and 5 μL of 3 mg mL^{-1} rutile TiO_2 mesocrystals suspension were deposed onto each holes in turn and also dried under infrared lamp. Repeat above step for three cycles to construct the hierarchically ordered MMMJ on ITO electrode. Subsequently, 250 mL of 4-MPBA functionalized Cu NCs was dropped on the electrode interface to obtain Cu NCs enhanced MMMJ. After treating by above steps, 250 μL of EDC/NHS was added to excite carboxyl group on 4-MPBA for 30 min since EDC/NHS activation was able to decrease energy barrier for carboxyl groups to react with amine (Peng et al., 2013). In succession, the insulated tape layer were removed with caution and the modified electrodes were immersed into 5 mL of 0.018 mg mL^{-1} LSR antibody solution and incubated for 50 min at room temperature. The LSR antibody was immobilized onto electrodes surface via classic EDC/NHS coupling reaction between amine groups on antibody and carboxyl group on 4-MPBA. After immobilization of LSR antibody, the electrodes were washed with PBS (pH 7.4) thoroughly to remove excessive antibody and followed by incubating with 1.0 wt% BSA for 40 min at 4 °C to block nonspecific sites. Finally, the electrodes prepared above were incubated with different concentration of LSR standard solution at 4 °C for 50 min and washed with PBS (pH 7.4) to remove physically adsorbed LSR.

2.5. Two-step PEC-colorimetric detection of LSR

For PEC measurements, the result electrode was immersed in PBS (pH 7.5) under an applied potential of 0.1 V. As for digital colorimetric analysis, the result electrode was dipped into the 0.6 wt% H_2O_2 solution which was diluted by PBS (pH 7.5), the prepared solution must blow with nitrogen to remove the dissolved oxygen before use. In this case, 0.6 wt% H_2O_2 solution was catalyzed by MMMJ under sustainably illumination with applied voltage of 1.5 V for 20 min and the result solution was dropped in the Leuco-MB functionalized colorimetric film to have a chromogenic reaction. Finally, the raw photographs of colorimetric films were transformed into RGB images and chromaticity in films were recorded to have a digital colorimetric analysis.

3. Results and discussion

3.1. Excellent PEC properties of MMMJ

To evaluate PEC properties and explore the electrons transfer regulation on constructed MMMJ, a series of photocurrent measurements were conducted. As Fig. 1A showed, comparing with single anatase phase TiO_2 mesocrystals (A) (red line) or rutile phase TiO_2 mesocrystals (R) (green line), a distinct increased photocurrent response generated on P25 (mixture of 80% anatase and 20% rutile TiO_2) and anatase/rutile mix TiO_2 mesocrystals junction (AR) (black line and blue line). By contrast, AR presented considerately enhanced photocurrent response

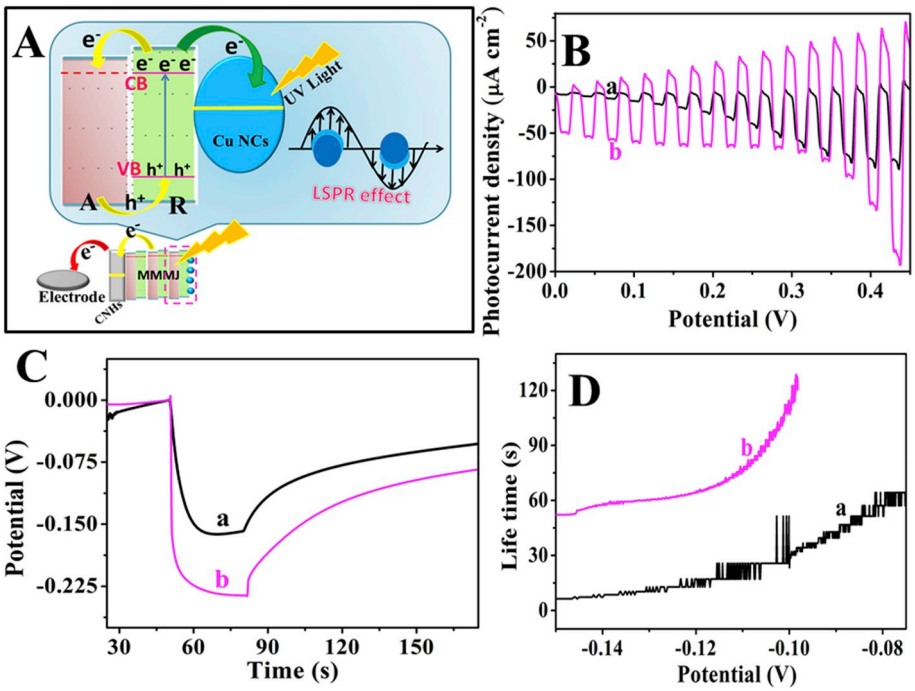

Fig. 2. (A) Sensitive mechanism of Cu NCs (B) Applied potential bias-dependent photocurrent densities (C) Voc time profile and (D) electron lifetime measurements (determined from the Voc decay in the dark) of (a) CNHs/MMMJ and (b) CNHs/MMMJ/Cu NCs in PBS (pH 7.5) with applied potential of 0.1 V.

than P25 since built-in potential distribution in hierarchically ordered structure drove electrons and holes toward desired directions. In this work, the band gap stagger and conductive band aligned may be two main band alignment types (staggered and conductive band aligned), which have been verified in previous researches (Zhang and Dong 2019). And Fig. 1B described two main band alignment type. As exhibited in type I, the Fermi level of rutile TiO_2 (0.167V) was higher than that in anatase TiO_2 (0.038V) (Cao et al., 2016). Under illumination, the photo-excited electrons on rutile TiO_2 mesocrystals tended to migrate to anatase TiO_2 mesocrystals so that their Fermi levels could keep equal. At the same time, photo-generated holes in anatase TiO_2 mesocrystals also had a tendency to transfer to rutile TiO_2 mesocrystals. As displayed in type II, the conductive band of anatase and rutile were aligned and the photo-generate electrons could migrate to both anatase and rutile. And two types of band alignment effect photocurrent generation simultaneously. As a proof-of-concept application, Fig. S4 exhibited the photocurrent responses on rutile/anatase mix TiO_2 mesocrystals junction (RA) (black) and AR (red). Both RA and AR exhibited positive photocurrent response, implying there may be two different charge carriers transfer directions (I and II) exited on anatase and rutile mix phase array. And a stronger photocurrent response was observed in AR for numerous of active holes aggregated on the rutile TiO_2 surface and these photo-generated holes were scavenged by electrons donors which efficiently inhibited recombination of electron-hole pairs. This result demonstrated that the influence of type I was dominant and type II was secondary. Inspired by this, as illustrated in Fig. 1C, a facile fabricated MMMJ was constructed just by coating more hierarchically ordered AR layers on electrode interface. The staggered band gap between different phase layers drove electrons and holes toward the desired direction. On the other hand, abundant of photo-generate electrons migrated on aligned conductive band inexhaustibly, which remarkably accelerated the electron migration to prolonged the electron life time (Jia et al., 2018; Jia et al., 2018; Zhang and Dong 2019). As illustrated in Fig. 1D, the synergetic effect between multiple AR layers in MMMJ caused multiple amplification of signal to generate more brilliant photocurrent responses. The photocurrent output reached top after three coating numbers of AR layers $(AR)_3$ (red line) and level off at four cycles modification of AR layers $(AR)_4$ (green line) since excessive semiconductor caused surface recombination and blocked the channel of charge transfer. Hence $(AR)_3$ was finally selected as the optimal modification layer of MMMJ.

It was worth mentioning that such a unique mixed phase junction constructing strategy was also successfully applied in ordinary TiO_2 nanoparticles. As indicated in Fig. S5, an enhanced photocurrent density displayed in the Anatase/RutileTiO_2 junction (A'R') (red line) compared to P25 (green line). And further increased photocurrent response generated after multiple anatase/rutileTiO_2 junction (A'R'A'R') (blue line) attached onto the electrode. Thus, these results discussed above provided a valuable guidance for designing more effective mixed phase junctions with excellent PEC performance.

3.2. Enhanced PEC performance in MMMJ based sensing platform

Cu NCs play a critical role in improving PEC properties of semiconductor owing to their small size, LSPR effect and boosting electrical conductivity (Nasrin et al., 2018; Li et al., 2017). Fig. 2A described the possible mechanism, under light irradiation, a great amount of excited electrons generated from valence band (VB) of MMMJ and jumped to conduction band (CB) of MMMJ. In this case, excited CB electrons in rutile TiO_2 mesocrystals could inject to anatase TiO_2 mesocrystals facilely. And part of CB electrons migrated to CuNCs for LSPR effect generated a strong near-field amplitude around the CuNCs, what could trap electrons from semiconductor materials and facilitated the electron-hole pairs separation on MMMJ (Liu et al., 2015; Shi et al., 2015, 2018). To confirm this supposition, as exhibited in Fig. 2B, an apparently enhanced photocurrent density generated in Cu NCs enhanced MMMJ (curve b) compared to MMMJ (curve a) under applied potentials from 0V to 0.4V. Furthermore, the typical open-circuit voltage (Voc) changes of MMMJ before (curve a) and after (curve b) modified with Cu NCs under visible light illumination were also evaluated to explore the recombination kinetics. As presented in Fig. 2C, when the light was on, a large number of electrons accumulated on electrode interface, causing a sharply negative shift of Fermi level. Following, the Voc value reached minimum and kept stable because of a

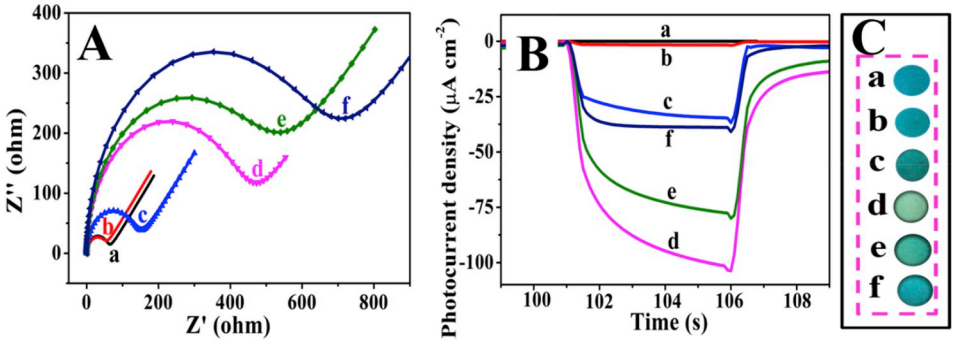

Fig. 3. The EIS (A), photocurrent (B) of different electrodes (a) bare electrode (b) electrode/CNHs (c) electrode/CNHs/MMMJ (d) electrode/CNHs/MMMJ/Cu NCs (e) electrode/CNHs/MMMJ/Cu NCs/anit-LSR (f) electrode/CNHs/MMMJ/Cu NCs/anit-LSR/LSR. (C) The raw photograph in corresponding colorimetric films. The photocurrent measurement was carried out in PBS (pH 7.5) with applied potential of 0.1 V. And electrochemical impedance were determined in mixed solution of 5.0 mM $K_3[Fe(CN)_6]/K_4[Fe(CN)_6]$ (1:1) containing 0.1 M KCl. The catalysis of H_2O_2 was carried out in PBS (pH 7.5) under sustainably illumination with applied voltage of 1.5 V for 20 min.

balance between electrons accumulation and charge recombination on electrode interface. However, once the light was switch off, the Voc decayed gradually due to the recombination of electron-hole pairs and scavenging of free electrons by electron acceptor species in the electrolyte. And by comparison, the Cu NCs enhanced MMMJ performed a more negative Voc value and slower Voc decline. Afterwards, the open-circuit voltage after stopping the illumination was further investigated by using the approximation derived based on Bisquert, which directly related to the electron lifetime by the following equation (Song et al., 2008)

$$\tau = \frac{k_B T}{e}\left(\frac{dV_{OC}}{dt}\right)^{-1} \quad (1)$$

Where τ was the potential dependent lifetime, k_B was Boltzmann's constant, T was the temperature in K, e was the charge of a single electron, and Voc was the open-circuit voltage at time t. As depicted in Fig. 2D, it could be distinctively told that the accumulated electrons on Cu NCs enhanced MMMJ (curve b) possessed a longer decay lifetime compare to MMMJ (curve a). Consequently, these results discussed above all confirmed significant sensitizing effect caused by Cu NCs.

3.3. Characterization of the immunosensor

In ordered to monitor the interfacial properties of surface-modified electrodes, the electrochemical impedance spectroscopy (EIS) on electrodes of each assembly steps were measured. The semicircle diameter was equal to transfer resistance, which reflected the electron transfer kinetics at the electrode interface. As shown in Fig. 3A, the bare electrode (curve a) displayed a slight hemicycle, meaning a clear electrode has obtained. And the transfer resistance (R_{et}) slightly decreased with the deposition of CNHs (curve b) for outstanding conductivity of CNHs accelerated electron transmission on electrode interface. When MMMJ modified onto the electrode, semicircle diameter apparently increased (curve c), which was ascribed to semiconductor properties of MMMJ hindered the transfer access of free electrons to electrode. After introduction of 4-MPBA modified Cu NCs (curve d), the large steric hindrance of 4-MPBA seriously interrupted the electrons migration channel, as a result, the electrochemical impedance was dramatically increased. And it could be distinctively told that the incubation of LSR antibody and LSR (curve e and f) lead to a further amplified transfer resistance owing to formation of insulating protein complex hindered the electron transmission on electrode interface.

The photocurrent response was another effective method to

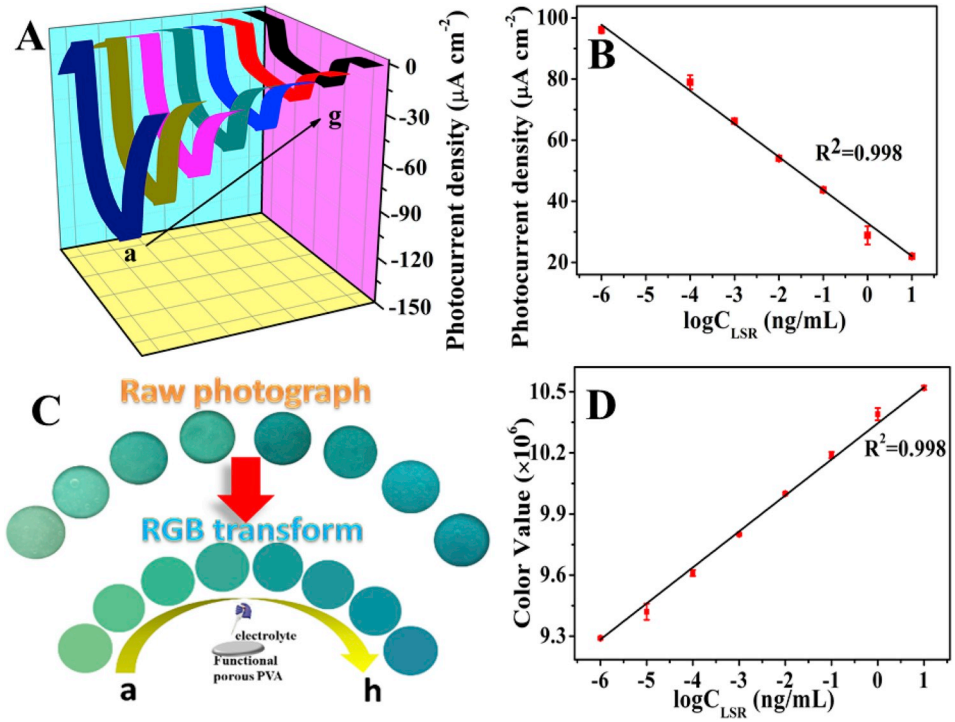

Fig. 4. Photocurrent responses (A) and corresponding calibration curves (B) of the PEC biosensor toward different concentrations of LSR. Color variations in lecuo-MB functionalized colorimetric PVA films (C) and corresponding calibration curves (D) of the colorimetric biosensor toward different concentrations of LSR. The photocurrent measurement was carried out in PBS (pH 7.5) with applied potential of 0.1 V. The catalysis of H_2O_2 was performed in PBS (pH 7.5) under sustainably illumination with applied voltage of 1.5 V for 20 min. (For interpretation of the references to color in this figure legend, the reader is referred to the Web version of this article.)

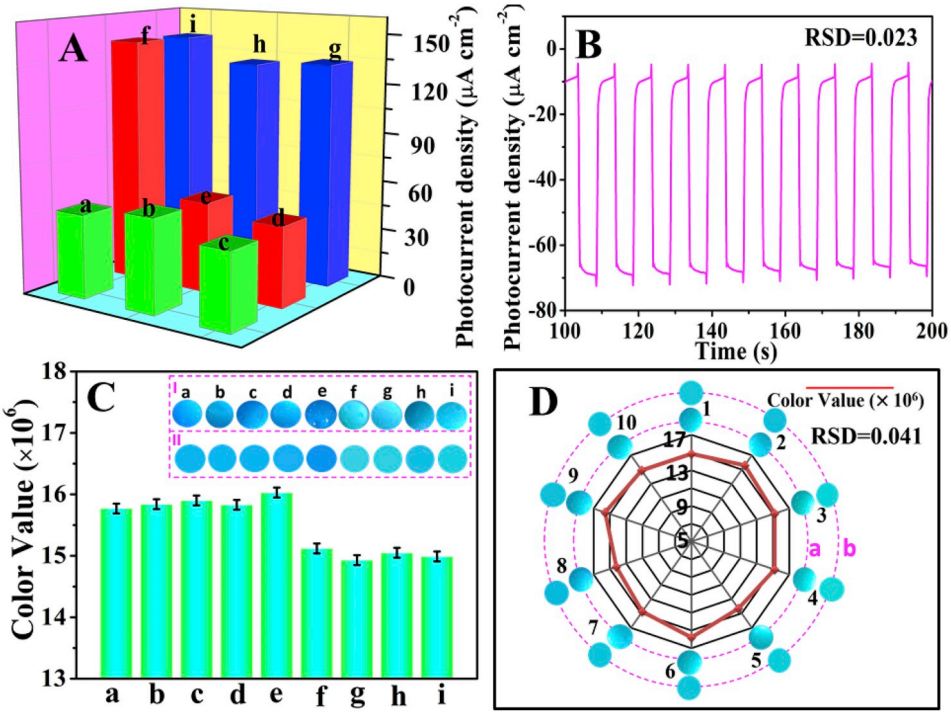

Fig. 5. Selectivity of the biosensor towards photocurrent density (A) and color value (C) was evaluated by comparing it to distractors at concentration of 1×10^{-2} ng/mL: 1×10^{-4} ng/mL LSR + HE4 (column a), 1×10^{-4} ng/mL LSR + AFP (column b), 1×10^{-4} ng/mL LSR + HPV16 E6 (column c), 1×10^{-4} ng/mL LSR (column d), mixture (column e), HE_4 (column f), AFP (column g), HPV16 E6 (column h), Blank (column i), the insert I and II in (C) were raw photograph and RGB photograph of colorimetric films respectively. (B) Ten parallel measurements of photocurrent output on one electrode/CNHs/ARARAR/Cu NCs in PBS (pH 7.5) with applied potential of 0.1 V. (D) Ten parallel measurements of color value on the lecuo-MB functionalized colorimetric PVA films, the circle **a** was raw photograph and circle **b** was RGB photograph. The photocurrent measurement was carried out in PBS (pH 7.5) with applied potential of 0.1 V. The catalysis of H_2O_2 was carried out in PBS (pH 7.5) under sustainably illumination with applied voltage of 1.5 V for 20 min.. (For interpretation of the references to color in this figure legend, the reader is referred to the Web version of this article.)

investigate fabrication procedure of the immunosensor. As Fig. 3B displayed, the photocurrent responses on bare electrode (curve a) and electrode/CNHs (curve b) were negligible. However, after coating with MMMJ, an evident photocurrent response generated on obtained electrode/CNHs/MMMJ (curve c) for well match energy levels between different phases considerately promoted the electron migration rate. And as expected, the photocurrent response enhanced dramatically with the introduction of Cu NCs owed to boosting electrical conductivity and LSPR effect of Cu NCs that significantly prolonged electron lifetime on electrode interface. Finally, as could be found in curve e and f, when LSR antibody and LSR incubated in ordered, the photocurrent decreased hugely, which implied that insulated protein complex have successfully anchored onto the electrode thereby blocked the channel of electron transfer. As for Fig. 4C presented the chromaticity in various colorimetric films after being oxidized with H_2O_2 solution what has been decomposed by different electrodes after each assembly step. It can be facilely told that the color intensity in different colorimetric films were corresponding to photocurrent intensities on different electrode interfaces. Hence, these results reasonably demonstrate the successful fabrication of the PEC-colorimetric immunosensor.

3.4. Analytical performance of the two-step PEC-colorimetric sensing system

To achieve the best sensing performance for LSR test, many important parameters such as concentration of different nanomaterials (CNHs, anatase TiO_2 mesocrystals, rutile TiO_2 mesocrystals and Cu NC), incubation time of antibody and antigen, pH and applied potential were all investigated (Figs. S7 and S8). Under optimum conditions, the photocurrent decrease with raising LSR concentration from a to g in Fig. 4A for absorption of insulation protein complex quenched the photocurrent signal on electrode. And Fig. 4B revealed the linear-dependence of photocurrent density to the logarithm of LSR concentration in the range between 10^{-6} ng/mL and 10 ng/mL, the regression equation was Photocurrent density (μA cm^{-2}) = −10.82 $logC_{LSR}$ (ng/mL) +32.87 ($R^2 = 0.998$) with a detection limit of 10^{-6} ng/mL. To have a colorimetric analysis, the result electrode was utilized as a photoanode to decompose 0.6 wt% H_2O_2 solution and the result solution was dropped into the Leuco-MB functionalized colorimetric film to allow the chromogenic reaction in progress. In succession, the digital colorimetric analysis was carried out by transforming the raw photograph of corresponding colorimetric films into RGB (red green and blue) image and recording variation in color intensity which can be characterized by the following equation:

Color value = red value + green value × 256 + blue value × 65536.

According to previous statements, the increased concentration of LSR on electrode interface inhibited catalytic decomposition of H_2O_2, thereby causing more lecuo-MB oxidized into blue MB. Therefore, as displayed in Fig. 4C and D, the various color intensity in colorimetric films can be observed with the naked eye and were also proportional to the target LSR concentrations in the range between 10^{-6} ng/mL and 10 ng/mL, which may provide an important reference for PEC measurement and effectively reduce false results. The regression equation could be expressed as Color value = 0.18 $logC_{LSR}$ (ng/mL) +10.34 ($R^2 = 0.998$) with a detection limit of 10^{-6} ng/mL. By merits of brilliant PEC properties and unique catalysis activity of MMMJ, the designed PEC-colorimetric biosensor for LSR detection performed a wider liner range and lower detection limit compared with other methods for OC biomarkers (Qian et al., 2013) detection as presented in Table S1.

3.5. Specificity, reproducibility, and stability of the two-step PEC-colorimetric biosensor

Furthermore, the specificity of PEC immunosensor was verified by using HE4, AFP and HPV16 E6 as possible interfering agents at an excess hundred folds concentration of LSR. As depicted in Fig. 5A the photocurrent response in presence of LSR (LSR + HE4 (a), LSR + AFP (b), LSR + HPV16E6 (c), LSR (d) and Mixture (e)) were much lower than that in the absence of LSR (HE4 (f), AFP (g), HPV16E6 (h) and blank (i)). And as expected in Fig. 5C, in the presence of LSR (columns a b c d e) the color intensity on colorimetric films were higher than that in the absence of LSR (columns f g i h) for that LSR immobilized on electrode interface weaked catalytic activity of MMMJ. Therefore, more H_2O_2 remained in solution accelerate oxidization of lecuo-MB to generate blue MB. Additionally, as demonstrated in Fig. 5B the photocurrent response on one electrode (electrode/CNHs/MMMJ/Cu NCs/Ab) was determined under

Table 1
Recovery measurements of LSR in human serum sample (n = 3).

Sample	Found (ng/mL)	Add (ng/mL)	Total found (ng/mL)	Recovery (%)
1	3.71×10^{-6}	blank	3.71×10^{-6}	
2	3.71×10^{-6}	0.1	0.100722	100.7
3	3.71×10^{-6}	0.01	0.010079	100.8
4	3.71×10^{-6}	0.001	0.000988	98.4

interrupted light irradiations and no distinctive decline of photocurrent was observed. In Fig. 5D, ten parallel color intensity measurements were carried out by treating the colorimetric films with H_2O_2 solution, which has been catalyzed by one electrode/CNHs/MMMJ/Cu NCs/Ab in PBS (pH 7.5) with applied potential of 0.1 V, there was no apparent difference on color values in each colorimetric film. The relative standard deviation (RSD) of photocurrent response and the color value in colorimetric films were 2.3% (Figs. 5B) and 4.1% (Fig. 5D) respectively. To evaluate the reproducibility of designed PEC biosensor, photocurrent response on four electrodes (electrode/CNHs/MMMJ/Cu NCs/Ab) were determined under interrupted light irradiations and then used as photoanodes to catalyze H_2O_2 in PBS (pH 7.5) under applied potential of 0.1 V. As displayed in Fig. S6 A, the RSD of four parallel experiments were 1.87%, 2.16%, 3.42% and 2.54% respectively. And as indicated in Fig. S6 B, there was no obviously difference between four corresponding colorimetric films. These results discussed above confirmed that the designed PEC possessed favorable stability and reproducibility. For a further investigate of practical analytical performance of designed biosensor, a human serum sample was added with 0.1, 0.01 and 0.001 ng/mL LSR. The result in Table 1 indicated that the recovery of the added LSR was in the range from 98.4% to 100.7%, which indicated superior precision of this biosensor and may have great promising potential for practical applications.

4. Conclusion

In summary, a series of experiments were performed to verify that LSR may be used as a new candidate biomarker for ovarian cancer early diagnosis. A versatile two-step PEC-colorimetric strategy was developed to realize ultrasensitive detection of LSR with an innovative MMMJ based sensing platform. Owing to the facile prepared progress and effective combination of photoactive layer, CuNCs enhanced MMMJ presented excellent PEC properties and high efficient catalytic activity to H_2O_2. The lecuo-MB acted as a color change reporter molecule can be efficiently oxidized by H_2O_2 from colorless to blue and observed with naked eye facilely. On the basic of this, a visual colorimetric analysis was introduced to reduce the false positive results during the measurement. Benefiting from unique fabricating progress and brilliant PEC properties of CuNCs enhanced MMMJ, the designed PEC-colorimetric biosensor exhibited high efficiency, superior sensitivity and satisfied specify for LSR monitoring, which may provide a value reference for construction of other sensing platforms and shed light on reliable prediction for other diseases.

Declaration of competing interest

The authors declare that they have no known competing financial interests or personal relationships that could have appeared to influence the work reported in this paper.

CRediT authorship contribution statement

Yanjie Chen: Investigation, Writing - original draft. **Shupei Zhang:** Writing - original draft. **Hong Dai:** Funding acquisition, Methodology, Project administration. **Zhensheng Hong:** Formal analysis. **Yanyu Lin:** Data curation, Formal analysis.

Acknowledgment

This project was financially supported by the NSFC (21877012, 21575024), National Science Foundation of Fujian Province (2016J06003, 2017J01620) and Education Department of Fujian Province (JK2016009, FBJG20170186,JA14071) was also greatly acknowledged.

Appendix A. Supplementary data

Supplementary data to this article can be found online at https://doi.org/10.1016/j.bios.2019.111809.

References

Cao, F.R., Xiong, J., Wu, F.L., Liu, Q., Shi, Z.W., Yu, Y.H., Wang, X.D., Li, L., 2016. ACS Appl. Mater. Interfaces 8, 12239–12245.
Cui, M.L., Zhao, Y., Song, Q.J., 2014. Trends Anal. Chem. 57, 73–83.
Dai, H., Zhang, S.P., Gong, L.S., Li, Y.L., Xu, G.F., Lin, Y.Y., Hong, Z.S., 2015. Biosens. Bioelectron. 72, 18–24.
Dai, H., Zhang, S.P., Hong, Z.S., Li, X.H., Xu, G.F., L, Y.Y., Chen, G.N., 2014. Anal. Chem. 86, 6418–6424.
Ding, E., Hai, J., Chen, F.J., Wang, B.D., 2018. ACS Appl. Nano Mater. 1, 4156–4163.
Hao, Q., Shan, X.N., Lei, J.P., Zang, Y., Yang, Q.H., Ju, H.X., 2016. Chem. Sci. 7, 774–780.
Hiramatsu, K., Serada, S., Enomoto, T., Takahashi, Y., Nakagawa, S., Nojima, S., Morimoto, A., Matsuzaki, S., Yokoyama, T., Takahashi, T., 2018. Cancer Res. 78, 516–527.
Jia, C.C., Zhang, X., Yang, P., 2018. Appl. Surf. Sci. 430, 457–465.
Jin, L.H., Zhang, Z.H., Tang, A., Li, C., Shen, Y.H., 2016. Biosens. Bioelectron. 79, 108–113.
Jin, S., Chen, M., Dong, H.F., He, B.Y., Lu, H.T., Su, L., Dai, W.H., Zhang, Q.C., Zhang, X. J., 2015. J. Power Sources 274, 1173–1179.
Kalinichev, A.V., Pokhvishcheva, N.V., Peshkova, M.A., 2019. Talanta 197, 638–644.
Li, N.T., Lu, Y.L., Li, S., Zhang, Q., Wu, J.J., Jiang, J., Liu, G.L., Liu, Q.J., 2017. Biosens. Bioelectron. 93, 241–249.
Liu, C.J., Yang, Y.H., Li, W.Z., Li, J., Li, Y.M., Chen, Q.Y., 2016. Chem. Eng. J. 302, 717–724.
Liu, E.Z., Qi, L.L., Bian, J.J., Chen, Y.H., Hu, X.Y., Fan, J., Liu, H.C., Zhu, C.J., Wang, Q. P., 2015. Mater. Res. Bull. 68, 203–209.
Liu, H.Y., Zhu, J.J., 2013. Chin. J. Anal. Chem. 41, 658–663.
Miao, Z., Hou, W.L., Liu, M.L., Zhang, Y.Y., Yao, S.Z., 2018. New J. Chem. 42, 1446–1456.
Nasrin, F., Chowdhury, A.D., Takemura, K., Lee, J., Adegoke, O., Deo, V.K., Abe, F., Suzuki, T., Park, E.Y., 2018. Biosens. Bioelectron. 122, 16–24.
Peng, J.M., Su, Y.L., Chen, W.J., Zhao, X.T., Jiang, Z.G., Dong, Y.N., Zhang, Y., Liu, J.Z., Cao, X.Z., 2013. J. Membr. Sci. 427, 92–100.
Qian, Y., Wang, Y., Zhang, X., Zhou, L., Zhang, Z., Xu, J., Ruan, Y., Ren, S., Xu, C., Gu, J., 2013. J. Proteome Res. 12, 4046–4055.
Ren, H., German, S.R., Edwards, M.A., Chen, Q.J., White, H.S., 2017. J. Phys. Chem. Lett. 8, 2450–2454.
Shinagare, A.B., Balthazar, P., Ip, I.K., Lacson, R., Liu, J., Ramaiya, N., Khorasani, R., 2018. J. Am. Coll. Radiol. 15, 1133–1138.
Su, Z., Graybill, W.S., Zhu, Y., 2013. Clin. Chim. Acta 415, 341–345.
Su, R., Bechstein, R., Sø, L., Vang, R.T., Sillassen, M., Esbornsson, B.r., Palmqvist, A., Besenbacher, F., 2011. J. Phys. Chem. C 115, 24287–24292.
Shi, Y., Wang, J., Wang, C., Zhai, T.T., Bao, W.J., Xu, J.J., Xia, X.H., Chen, H.Y., 2015. J. Am. Chem. Soc. 137, 7365–7370.
Shi, Yi, Zhang, Q., Zhai, T.T., Zhou, Y., Yang, D., 2018. Electrochim. Acta 271, 361–369.
Song, X.M., Wu, J.M., Tang, M.Z., Qi, B., Yan, M., 2008. J. Phys. Chem. C 112, 19484–19492.
Wei, J., Chang, W.D., Qileng, A., Liu, W.P., Zhang, Y., Rong, S.Y., Lei, H.T., Liu, Y.J., 2018. Anal. Chem. 90, 9606–9613.
Yan, B.D., Z, Y., Jiang, Y.L., Xu, W., Chen, Y.J., Tu, J.C., Wang, X.H., Wu, Q., 2018. Appl. Surf. Sci. 458, 382–388.
Zhang, D.Y., Dong, S.A., 2019. Prog. Nat. Sci.: Mater. Int. 29, 277–284.